In-plane silicon probes for simultaneous neural recording and drug delivery



2010 J. Micromech. Microeng. 20 105006

(http://iopscience.iop.org/0960-1317/20/10/105006)

J. Micromech. Microeng. **20** (2010) 105006 (11pp) doi:10.1088/0960-1317/20/10/105006

# In-plane silicon probes for simultaneous neural recording and drug delivery

**K Seidl[1], S Spieth[2], S Herwik[1], J Steigert[3], R Zengerle[2,3], O Paul[1] and P Ruther[1]**

[1] Microsystem Materials Laboratory, Department of Microsystems Engineering (IMTEK), University of Freiburg, Freiburg, Germany
[2] Institut für Mikro- und Informationstechnik der Hahn-Schickard-Gesellschaft eV (HSG-IMIT), Villingen-Schwenningen, Germany
[3] Laboratory for MEMS Applications, Department of Microsystems Engineering (IMTEK), University of Freiburg, Freiburg, Germany

E-mail: seidl@imtek.de

Received 9 June 2010, in final form 9 July 2010
Published 3 September 2010
Online at stacks.iop.org/JMM/20/105006

**Abstract**
This paper reports on the design, fabrication and characterization of silicon-based microprobes for simultaneous neural recording and drug delivery. The fabrication technology is based on two-stage deep reactive ion etching combined with silicon wafer bonding and grinding to realize channel structures integrated in needle-like probe shafts. Liquids can be supplied to microfluidic devices via in-plane and out-of-plane ports. The liquid is dispensed at circular out-of-plane ports with a diameter of 25 $\mu$m and rectangular in-plane ports with dimensions of $50 \times 50$ $\mu$m$^2$. Two-shaft probes with a pitch between shafts of 1.0 and 1.5 mm were realized. The probe shafts have a length of 8 mm and rectangular cross-sections of $w \times h$ ($w = 250$ $\mu$m and $h = 200$ or 250 $\mu$m). Each shaft contains one or two fluidic channels with a cross-section of $50 \times 50$ $\mu$m$^2$. In addition, each probe shaft comprises four recording sites with diameters of 20 $\mu$m close to the outlet ports. Mechanical and fluidic characterization demonstrated the functionality of the probes. Typical infusion rates of 1.5 $\mu$L min$^{-1}$ are achieved at a differential pressure of 1 kPa. The Pt-gray electrodes have an average electrode impedance of $260 \pm 59$ k$\Omega$ at 1 kHz.

## 1. Introduction

The complex interactions of large neural networks with impressive numbers of neurons through electrical and chemical signals are still under investigation and a challenging research topic in neuroscience. Tools combining the capability of neural recording with a well-defined drug delivery close to the recording site offer interesting perspectives addressing some of these challenges. Dispensed drugs can be used (i) for chemical stimulation or inactivation of synaptic activity [1, 2], (ii) to suppress unintended reactions of brain tissue, e.g. inflammatory reactions [3], (iii) as imaging tracers [4] and (iv) for *in vivo* calibration of biosensors [5]. The availability of such probes opens new perspectives in research and application, e.g. in neural prostheses, as well as for the diagnosis and therapy of neurodegenerative brain diseases including Alzheimer's and Parkinson's diseases, neural dysfunctions such as epilepsy and neural degeneration, i.e. tumors.

Previously, research efforts have focused mainly on the investigation of electrical cell communication using the extracellular recording of neural activity of single neurons or clusters of neurons [6–9]. In the first case, one speaks of single unit activity (SUA). In the case of neuron clusters, multiple unit activity (MUA) and local field potentials (LFP) can be recorded. Ideally, neural devices making such recordings possible have the following features and properties: precise and reproducible electrode configurations[4,5], high resolution by a large number of closely spaced electrodes [10], affordable fabrication costs[4,5] and the possibility to integrate electronics

[4] NeuroNexus Technologies, 3985 Research Park Dr Suite 100, Ann Arbor, MI 480108, USA.
[5] Blackrock Microsystems, Salt Lake City, UT, USA.

 

[10] and additional microsensors such as biosensors to detect L-glutamate and choline [11]. It is further required that these devices are biocompatible and applicable in long-term recordings.

Currently, these requirements can be satisfied only using silicon-based arrays with slender probe shafts comprising multiple electrodes arranged in one-dimensional (1D) [9, 12, 13], 2D [9, 13, 14] and 3D [15–18] electrode configurations fabricated using microsystem technologies. These arrays implement either an in-plane approach [9, 12] with possible assembly into 3D arrays [13, 15–18] or an out-of-plane approach with silicon needles comprising a single recording site at the needle tip [16].

State-of-the-art pressure-driven drug delivery in neuroscience is performed mainly using stainless steel or glass capillaries with inner diameters down to 40 $\mu$m and a corresponding outer diameter of around 100 $\mu$m [19, 20] connected to flexible tubing and an external syringe pump. If neural recording in response to a dispensed liquid is required, separate wire electrodes are inserted into the brain tissue close to the dispensing needle. This, however, involves uncertainties in the relative positioning of dispensing and recording probes and limits the minimal distance between them. The distance between the fluidic ports and microelectrodes has been decreased using hybrid probes consisting of tungsten wire electrodes either attached to fused silica tubing [20] or passed through glass capillaries [21]. Alternative assemblies combining polymer and silicon microelectrode arrays glued to fused silica tubes [22] were recently brought to the market by NeuroNexus Technologies[4]. Drawbacks of these hybrid probes are seen in a rather delicate assembly and the limited choice in drug release location. Currently, the release direction is restricted to the probe tip. Efforts have been made to overcome these limitations by combining electrical and fluidic functionality on microfabricated neural probes.

Microfluidic channels have been integrated into transdermal and neural needle arrays using (i) surface micromachining based on sacrificial layers, (ii) bulk micromachining followed by the sealing of small etch orifices and (iii) bonding techniques. In the case of surface micromachining, the channel geometry has been defined using sacrificial materials such as phosphosilicate glass (PSG) [23] and thick photoresists [19, 24–26]. The sacrificial structure is covered by a thin film consisting of silicon nitride [24, 25], nickel and palladium [25, 26], or parylene [19] as schematically shown in figure 1(*a*). Etch openings are patterned into these layers so that the sacrificial material is selectively removed from the channel structures. A factor limiting the cross-sectional area of microfluidic structures realized using this approach is the mechanical stability of the cover layer. Additionally, the structure length is restricted by the diffusion-limited removal of the sacrificial materials.

Bulk micromachining based on anisotropic wet etching using ethylene-diamine pyrocatechol (EDP) [27] and potassium hydroxide (KOH) [28] solutions or using isotropic dry etching [29, 30] allows buried channel structures to be realized as illustrated in figures 1(*b*) and (*c*). Openings in

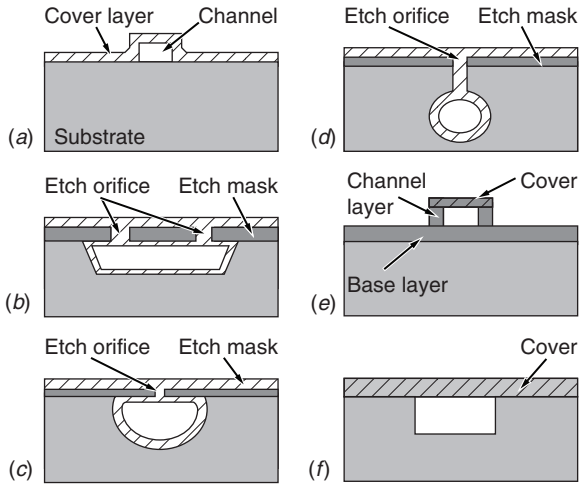


**Figure 1.** Various fabrication processes for fluidic channels using (*a*) surface micromachining, (*b*)–(*d*) bulk micromachining based on (*b*) wet or (*c*),(*d*) dry etching of silicon followed by the sealing of the etch orifices, (*e*),(*f*) bonding of polymer or silicon cover layers to channels (*e*) structured with an intermediate layer and (*f*) structured in the substrate.

the etch mask layer have to be subsequently sealed e.g. by depositing materials such as silicon oxide [27, 28]. The cross-sectional area of these channels is restricted by the diffusion-limited etch rate through the openings and the mechanical stability and hermeticity of the sealing layer. In addition, if anisotropic wet etching using KOH is applied, the channel layout is restricted to straight lines and bends of 90°. In order to etch fluidic channels with larger diameters starting from narrow etch openings, a combination of anisotropic and isotropic dry etching, as illustrated in figure 1(*d*), has been proposed [29, 31].

Further approaches to realize fluidic channels using bonding techniques have been based on surface or bulk micromachining. As an example, polymer-based neural probes have been realized by bonding an SU-8 cover onto SU-8 channel structures [32]. The channels have been generated by structuring a separate channel layer on an SU-8 base layer, as illustrated in figure 1(*e*). In contrast, gold–gold (Au–Au) thermocompression bonding of patterned titanium (Ti) shafts with channels to a Ti cover foil has been described in [33]. Similar approaches use the bonding of polydimethylsiloxane (PDMS) foils on silicon wafers [34], molds coated with parylene [35], glass wafers [36] and silicon-on-insulator (SOI) wafers [37] (see figure 1(*f*)). In the latter case, the channel structure is defined using deep reactive ion etching (DRIE) of silicon followed by silicon fusion bonding of a cover wafer. Major advantages are the design freedom in shaping the channel and the gas tightness owed to the applied silicon and silicon oxide. However, the SOI wafers used in this approach are relatively expensive.

Some of these fluidic devices were designed purely for dispensing liquids in various medical applications such as transdermal drug delivery [33, 38]. In contrast, other microprobes [27, 28, 31–34] are intended for use in neural applications relying on both microfluidic functionality and

neural recording. This goal is achieved by integrating microchannels and microelectrodes on the same probe shaft.

The work presented in this paper has been performed within the EU-funded *NeuroProbes* project [39–41] aiming at the development of multifunctional 1D, 2D and 3D neural probe arrays comprising passive [9, 13, 17] and active [10] recording electrodes, microfluidic functionality [42, 43] and amperometric biosensors for the detection of neurotransmitters, i.e. choline and L-glutamate [11]. This paper describes a novel probe concept offering the advantages of fluidic functionality with the in-plane and out-of-plane inlet and outlet ports combined with the simultaneous neural recording during drug dispensing. The design requirements and the system approach chosen for this study are described in section 2. The fabrication process used to realize microfluidic channel structures integrated in slender needle-like probe shafts is detailed in section 3. The selected technology is compatible with the process technologies used in the *NeuroProbes* project [9, 11]. It is based on two-stage DRIE combined with silicon wafer bonding and grinding. The mechanical probe characterization and insertion tests using a brain model as well as electrical and fluidic tests are reported in section 4.

## 2. Probe concept

### 2.1. Design requirements

Within the *NeuroProbes* project multifunctional microprobe arrays comprising electrodes for electrical recording and stimulation, biosensors and microfluidics have been developed [39–41]. For this reason, the fabrication of the fluidic microprobes was chosen to be compatible with fabrication processes and materials used in *NeuroProbes* [9]. These materials are silicon as the probe material and silicon oxide and nitride as passivation layers. Further, the fluidic probes were designed to be compatible with the modular approach pursued by *NeuroProbes* with the assembly of various probes into a platform [17]. As the probes are intended to perform injections in brain regions located at depths of 5 mm and more, a total probe length of about 8 mm was required. Further, two different liquids, e.g. a drug and a buffer reference, should be delivered with intended infusion volumes in the range of 0.5–0.75 $\mu$L per fluidic probe at flow rates of about 0.1–0.2 $\mu$L min$^{-1}$. In order to minimize the infusion pressure at these flow rates, a channel cross-section of 50 $\times$ 50 $\mu$m$^2$ was targeted.

### 2.2. System approach

Based on the fluidic and technological requirements, a fabrication process based on wafer bonding and dry etching of the fluidic probe structure was developed. As described in detail in section 3.2, the fluidic channels are structured into a channel wafer using a two-stage DRIE process followed by silicon wafer bonding, grinding of the cover wafer and finally double-sided DRIE. In this way, the fluidic structure is fabricated independently of its sealing. This results in a highly flexible design of the dimensions of the fluidic structures, i.e. the width, height and wall thickness of the channels. In view of the proper fluidic connection of the probe shaft to fluidic tubing and considering the necessary platform integration, it is beneficial to have the channel in the center of the probe shaft cross-section. A further advantage of the bonding technology is the possibility of coating the channel surface with a silicon oxide layer prior to wafer bonding. The wafer grinding allows the height of the channel cover to be adjusted and standard double-side-polished silicon substrates to be applied instead of the more expensive SOI wafers. In addition, as described below, the process offers high flexibility in positioning the fluidic outlet ports in the probe shaft. Similarly, the fluidic inlet ports can be placed either in-plane or out-of-plane with respect to the probe shaft.

## 3. Design and fabrication

### 3.1. Layout of fluidic microprobes

The neural microprobes with fluidic functionality are schematically shown in figure 2. They comprise two slender, needle-like probe shafts attached to a probe base for electrical and fluidic interconnection. Each shaft contains planar, circular electrodes and one or two microfluidic channels. The liquid may be supplied either in-plane through sockets at the probe base compatible with the platform concept of the *NeuroProbes* project. This is shown in figure 2(*a*). Alternatively, out-of-plane fluidic access ports can be made available at the bottom face of the probe base as shown in figure 2(*b*). The fluid is dispensed into the brain tissue via outlet ports on the shaft front surface in the out-of-plane direction (figure 2(*a*1)). A further probe variant comprises additionally outlet ports in the sidewalls of the probe shaft for in-plane fluid dispensing, as indicated in figure 2(*a*2). Four planar electrodes with an electrode area of 20 $\mu$m in diameter [9] are positioned upstream and downstream of the outlet port and connected by 20 $\mu$m wide leads with bonding pads on the probe base. In this study, the electrode pitch is 500 $\mu$m. The fluidic channels have a quadratic cross-section of 50 $\times$ 50 $\mu$m$^2$. Out-of-plane outlet ports are circular and measure 25 $\mu$m in diameter. In-plane outlet ports are 50$\times$50 $\mu$m$^2$ in size. The probe shaft is 250 $\mu$m wide with a thickness depending on the applied wafer grinding of the cover wafer and the rear DRIE etch process, as described in section 3.2. The standard shaft thickness is 250 $\mu$m; however, thicknesses down to 150 $\mu$m were realized as well. The sharp tip of the probe shaft has an opening angle of 17°. The 400 $\mu$m thick probe base measures 4 $\times$ 4 mm$^2$ or 4 $\times$ 6 mm$^2$ in the case of the in-plane and out-of-plane variants, respectively. It carries eight bonding pads (150$\times$300 $\mu$m$^2$) for wire bonding to a printed circuit board or for connecting highly flexible polyimide ribbon cables using the *Microflex Technology* [44]. For probe tracking, a wafer code (90 $\times$ 90 $\mu$m$^2$) [9] is integrated on each probe base. As summarized in table 1, seven different variants of neural probes with fluidic functionality were implemented.

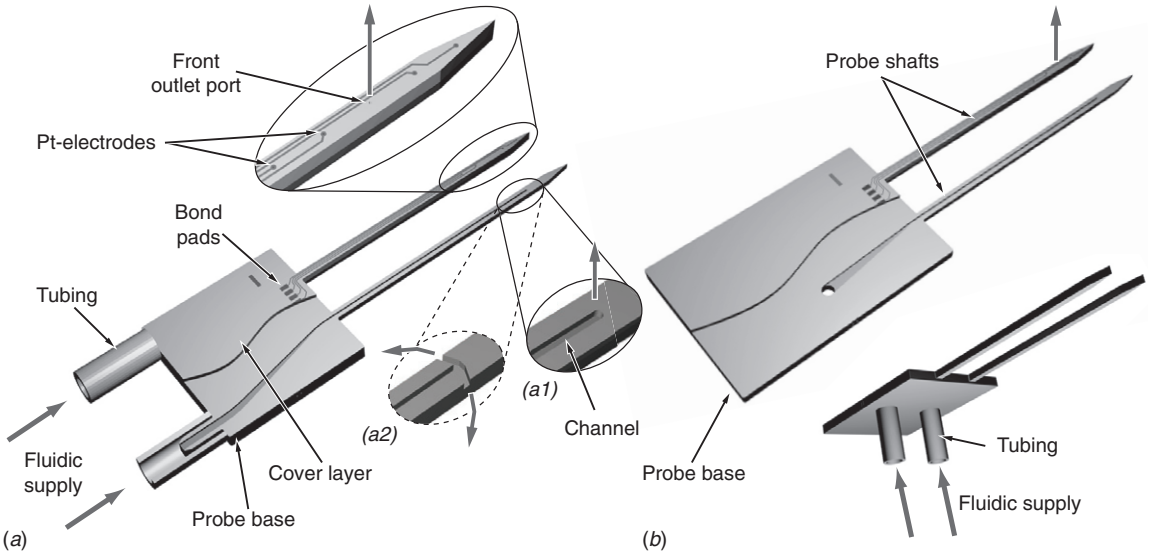


**Figure 2.** Exploded sectional views of neural probes with microfluidic functionality comprising (*a*) in-plane and (*b*) out-of-plane fluidic supply through polymer tubing. The fluidic inlet and outlet ports are indicated by bold arrows. Two different types of outlet ports are implemented: (*a*1) out-of-plane and (*a*2) in-plane.

**Table 1.** Variants of fluidic microprobes with corresponding layout parameters.

| Fluidic connection | Shaft pitch (mm) | Shaft length (mm) | Channels per shaft | Outlet ports per shaft | Outlet port location |
|---|---|---|---|---|---|
| In-plane | 1.5 | 8 | 1 | 1 | Front |
| | 1.5 | 6 | 1 | 1 | Front |
| | 1.0 | 8 | 1 | 1 | Front |
| | 1.5 | 8 | 2 | 2 | Front |
| | 1.0 | 8 | 1 | 3 | 1 × front, 2 × side |
| Out-of-plane | 1.5 | 8 | 1 | 1 | Front |
| | 1.5 | 8 | 2 | 2 | Front |

### *3.2. Fabrication process*

The fabrication process of passive silicon-based neural probes [9] developed in the framework of the *NeuroProbes* project was further extended to include fluidic channels. The nine-mask fabrication process is summarized in figure 3. It starts with the dry etching of 150 nm deep alignment marks on the rear of 300 $\mu$m thick, double-side-polished, 4 inch (1 0 0) wafers using dry etching as illustrated in figure 3(*a*). These marks ensure the precise alignment of all subsequent masks. This is followed by the thermal oxidation of the wafers providing a 300 nm thick protective layer on the wafer rear during the following dry etching steps.

*3.2.1. Fluidic channel patterning.* An additional 2 $\mu$m thick silicon oxide ($SiO_x$) layer is deposited on the front surface of the *channel wafer* using plasma-enhanced chemical vapor deposition (PECVD). It is then patterned by reactive ion etching (RIE) with the result schematically shown in figure 3(*b*). The $SiO_x$ layer serves as the masking layer against the subsequent two-stage DRIE process performed in an inductively coupled plasma (ICP) etcher (ICP Multiplex from STS, Newport, UK). The mask layout comprises the channel structure as well as the shape of the neural probes, i.e. shafts and probe base. In order to define the channel depth independently of the depth of the trenches delimiting the outer probe geometry, the mask openings for the channels are first covered by a photolithographically structured 5 $\mu$m thick photoresist (AZ4533, MicroChemicals GmbH, Germany) (figure 3(*b*)). The outer probe shape and out-of-plane fluidic connections are etched in a first DRIE step to a depth of 100 $\mu$m. After removal of the AZ4533 photoresist, the fluidic channels with a depth of 50 $\mu$m are defined in a second DRIE step (figure 3(*c*)). As a result, probe shape and out-of-plane fluidic connections are further etched to a total depth of 150 $\mu$m indicated in figure 3(*c*).

*3.2.2. Silicon wafer bonding and grinding.* The thermal oxide and PECVD oxides are then removed by wet etching. This is followed by thermal oxidation of either the channel wafer to an oxide thickness of 500 nm, the cover wafer (oxide thickness of 1000 nm) or both. These oxide layers serve as an etch stop for the subsequent DRIE steps to compensate for inhomogeneous etch rates over the wafer. If both channel and cover wafers are oxidized, the fluidic channel walls are completely passivated by oxide.

Prior to wafer-to-wafer bonding, both wafers are cleaned and treated to promote the formation of hydrophilic groups

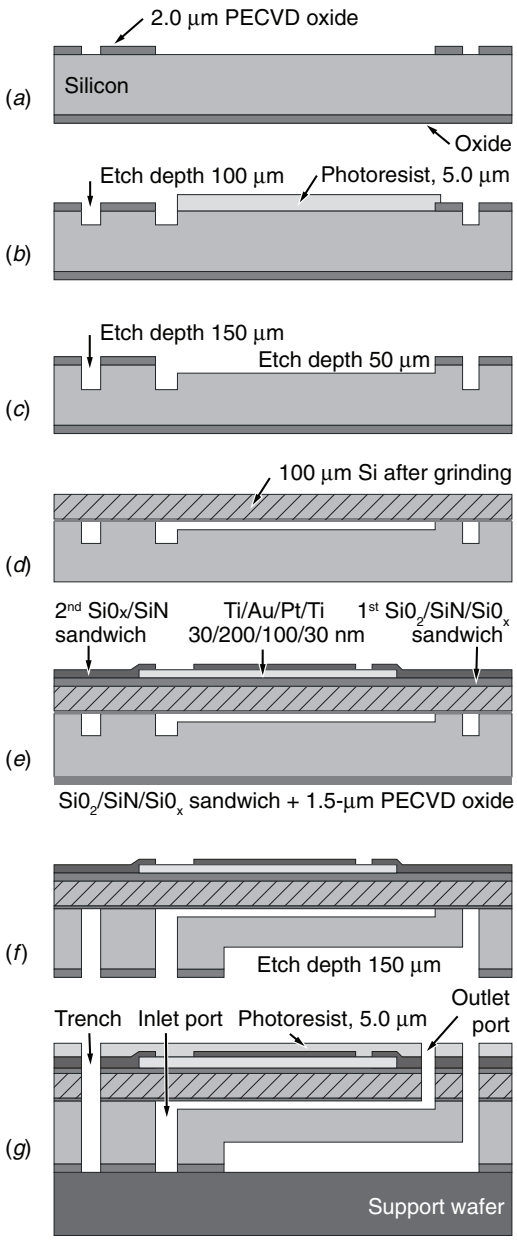


**Figure 3.** Fabrication process of silicon microprobes with fluidic functionality; (*a*) introduction of alignment structures, deposition and patterning of etch mask, (*b*), (*c*) two-stage DRIE process of channel structure, (*d*) wafer bonding and grinding, (*e*) isolation, electrode and pad metallization as well as passivation layer deposition and patterning, (*f*), rear and (*g*) front side DRIE for probe patterning.

on the wafer surfaces. Since the cover wafer is not structured before bonding, no wafer alignment is required. The wafers are bonded using direct wafer bonding at 1050 °C. The resulting wafer stack is illustrated in figure 3(*d*). During bonding, special precautions have to be taken to keep the pressure level inside the channel cavities low enough to be compatible with the subsequent DRIE steps in vacuum. The bonding step is followed by the thinning of the cover wafer using a commercial grinding and polishing process (see figure 3(*d*)) by Disco Hi-Tec Europe, Munich, Germany. To date, thicknesses of the cover wafer down to 50 $\mu$m were achieved. The resulting surface roughness of 14 nm is sufficiently low for further processing.

*3.2.3. Metallization.* The subsequent process steps are similar to those described in detail previously [9]. First, a stress-compensated layer sandwich consisting of 200 nm thick thermal oxide ($SiO_2$), 100 nm thick silicon nitride ($Si_xN_y$) produced by low pressure chemical vapor deposition (LPCVD), and 200 nm thick low temperature oxide (LTO) is deposited on both sides of the wafer stack. Next, a 1.5 $\mu$m thick PECVD $SiO_x$ layer is deposited on the wafer back. It serves as the etch mask against the subsequent DRIE step. The metallization of the electrodes, leads and bonding pads is realized using evaporation and lift-off of a gold/platinum (Au/Pt) layer stack, with the respective thicknesses of the Au and Pt layers of 200 nm and 100 nm. The Au layer is optional and reduces the resistance of the conducting lines. The metal stack is sandwiched between two 30 nm thick titanium (Ti) adhesion layers as illustrated in figure 3(*e*). The metallization is covered by a further stress compensated 1 $\mu$m thick PECVD $SiO_x/Si_xN_y$ layer stack. It is opened at the location of the electrodes and bonding pads using RIE in the RIE STS Multiplex etcher (cf figure 3(*e*)). The upper Ti on the Pt electrodes is removed in 1% hydrofluoric acid (HF) followed by an activity test using hydrogen peroxide [9].

*3.2.4. Probe patterning.* The rear dielectric layers, i.e. PECVD masking oxide and $SiO_2/Si_xN_y$/LTO layer stack, are patterned by RIE followed by a DRIE step with an etch depth of 150 $\mu$m using the STS ICP Multiplex etcher. A resulting cross-section is schematically shown in figure 3(*f*). This DRIE step defines the final shaft thickness, the overall probe shape as well as the out-of-plane fluidic supplies on the rear side of the wafer stack. Next, the dielectric layers on the front side, i.e. passivation and insulation layer stacks, are patterned by RIE. The subsequent DRIE step with an etch depth equivalent to the thickness of the cover wafer releases the probes. Thereby, the probes are suspended in the wafer stack by thin struts. A challenge for the DRIE is the etching of the out-of-plane fluidic outlet ports with diameters of 25 $\mu$m simultaneously with the 100 $\mu$m wide trenches defining the probe geometry. Due to RIE lag [45], the etch rate in the outlet ports is lower than in the trenches. RIE lag is well known to occur in cases where structures of different sizes and targeted aspect ratio have to be etched in parallel. As a consequence, the outlet ports require a longer etch time than the trenches, which results in trench over-etching. To avoid wafer fracture, the final DRIE process is performed on a support wafer, similar to the process described in [9].

The wafer stacks, i.e. the channel and cover wafer, constituting the fluidic probes are available in different variants defined by the thermal oxide growth on either channel or cover wafers or both (cf section 3.2.2). Technological consequences of the three cases are now discussed individually.

*Oxidized cover wafer.* When only the cover wafer is oxidized (cf figure 4(*a*1)), minor notching [46, 47] appears as soon as the rear and front DRIE reaches the cover wafer oxide (cf

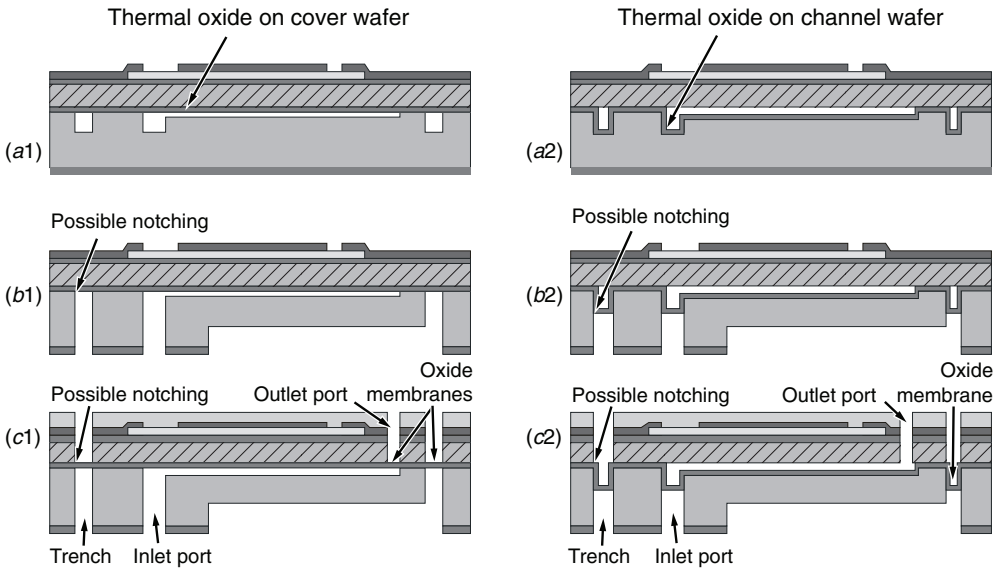


**Figure 4.** Final DRIE patterning of the wafer stack illustrating the effects of oxidized (*a*1)–(*c*1) cover or (*a*2)–(*c*2) channel wafers and the location of remaining oxide membranes in the etch trenches as well as in the fluidic inlet and outlet ports.

figures 4(*b*1), (*c*1)). Since a sufficient over-etching is required in view of the RIE lag, the SOI kit from STS was chosen to minimize notching. Advantage of a pulsed low frequency platen power supply is taken to reduce the ionic charging of the oxide layer [48]. The oxide membranes remaining in the etch trenches and in particular in the outlet ports schematically shown in figure 4(*c*1) have to be removed. Whereas front dry etching was successfully applied for 50 $\mu$m thin cover wafers, it failed in the case of cover wafers with a thickness of 100 $\mu$m. Wet etching using buffered HF is no option since the passivation layers of the probe shaft will be attacked as well. Removing the small oxide membranes in the outlet ports proved to be particularly challenging. It was found that they can be removed using either time-consuming argon ion beam etching or ultrasonic energy. For the latter approach, the membranes in the 100 $\mu$m wide trenches were first removed by RIE. Then, the probe channels were filled with isopropanol. Individual probes were then lowered into an ultrasonic bath (US) where the US energy caused the rupture of the oxide membranes in the out-of-plane outlet ports.

*Oxidized channel wafer*. When only the channel wafer was oxidized (cf figure 4(*a*2)), the rear DRIE causes notching at the thermal oxide of the channel wafer (cf figure 4(*b*2)). Again this effect can be minimized using the SOI kit of STS. The front DRIE cuts down into the existing trenches in the channel wafer as schematically shown in figure 4(*c*2). Again, the out-of-plane outlet ports require sufficient over-etching with minimal notching handled by the SOI kit. In contrast to the case with the oxidized cover wafer, all the remaining oxide membranes (cf figure 4(*c*2)) are located in the trenches and out-of-plane fluidic inlet ports. Thus, they have dimensions of at least 100 $\mu$m. As a consequence, they are removed using RIE from the wafer rear. For this purpose, the photoresist remaining after the rear side DRIE as well as the 1.5 $\mu$m thick passivation layer on the wafer rear serve as etch mask layers.

*Oxidized channel and cover wafer*. In the case both channel and cover wafers are thermally oxidized prior to wafer bonding, effects described in both preceding cases have to be taken into account. The major advantage resides in the fact that the entire surface of the resulting channels is oxidized. This improves the biocompatibility of the fluidic channels with respect to the used liquids.

Scanning electron micrographs of fluidic channels as well as the outlet and inlet ports are shown in figure 5. The corresponding locations of these details are indicated in the front view of the overall probe layout with out-of-plane and in-plane fluidic connections in figures 5(*a*) and (*e*), respectively. Figure 5(*b*) illustrates the resulting stepped etch profile of one probe shaft with two channels structured in the channel wafer. The tips of a completed fluidic probe with in-plane and out-of-plane outlet ports are shown in figure 5(*f*). An out-of-plane fluidic inlet port with the corresponding fluidic channel is given in a front view of a channel wafer in figure 5(*c*). The in-plane fluidic inlet port of a completed neural probe is shown in figure 5(*g*). The stepped sidewall indicates the interface between channel and cover wafers. The channel structures within the probe bases of the two probe types are given in figures 5(*d*) and (*h*). The thin struts of the probes for suspension in the wafer stack are highlighted. A photograph of a 4″ wafer after fabrication is shown in figure 6(*a*) with three probes removed for inspection. Minor striae resulting from wafer grinding are visible in figure 6(*b*). Details of completed fluidic probes with recording capability are compiled in figure 7. The electrodes are shown in figures 7(*a*) and (*b*). They are located in close proximity to the fluidic out-of-plane outlet port with a diameter of 25 $\mu$m (cf figure 7(*b*) and (*c*)). Figure 8 shows the example of a system assembly of a neural probe with two in-plane fluidic supplies. Two polytetrafluoroethylene (PTFE) tubings are attached to

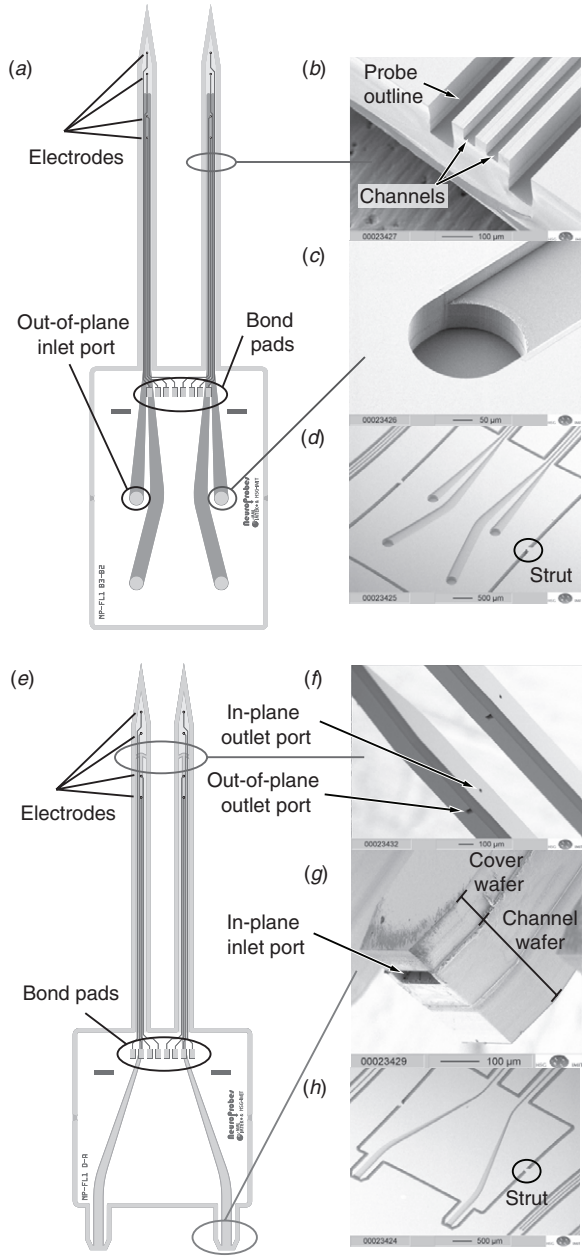


**Figure 5.** Layouts and scanning electron micrographs of (*a*)–(*d*) out-of-plane and (*e*)–(*h*) in-plane probes in comparison with the probe layout; (*a*), (*e*) front views of the overall probe layout, (*b*) front view of the diced channel wafer with stepped etch profile of one shaft with two channels and deeper probe outline, (*c*) front view of the channel wafer with etched fluidic out-of-plane inlet port, (*d*), (*h*) front views of the channel wafer with probe base containing channel structures and struts, (*f*) view of the tip of a completed neural probe with in-plane and out-of-plane outlet ports and (*g*) view of a completed neural probe with the fluidic in-plane inlet port.

the fluidic inlet ports of the silicon probe. The probe is then fixed to a polyetheretherketone (PEEK) package using an adhesive. A flexible printed circuit board (FPCB) with a conventional connector of 1.27 mm contact pitch is attached to the probe and its package. Finally, the probe is wire-bonded to the FPCB. Details on the assembly process are described elsewhere [43].

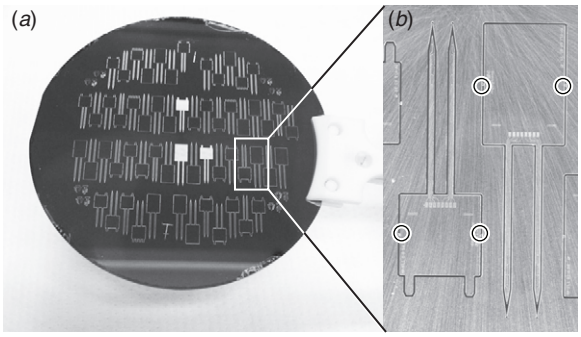


**Figure 6.** (*a*) Fabrication wafer with probes (three samples removed for inspection), (*b*) close-up with two fluidic microprobes suspended by thin struts indicated by circles.

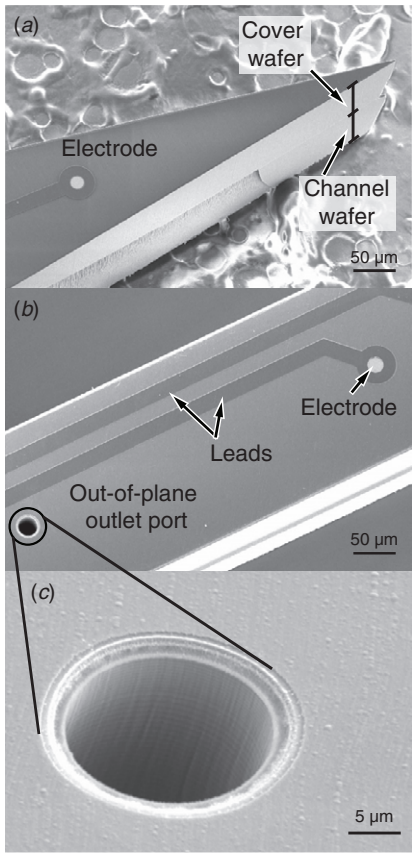


**Figure 7.** Scanning electron micrographs of fabricated fluidic microprobes: (*a*) tip of the microprobe with one electrode, (*b*) shaft with the out-of-plane outlet port close to an electrode and (*c*) close-up of the out-of-plane outlet port in (*b*).

## 4. Results

Initial mechanical, fluidic and electrical measurements performed using the new multifunctional neural probes are now described.

### *4.1. Mechanical characterization*

Silicon-based neural probes are known to withstand large forces of up to 500 mN applied along the shaft axis [41].

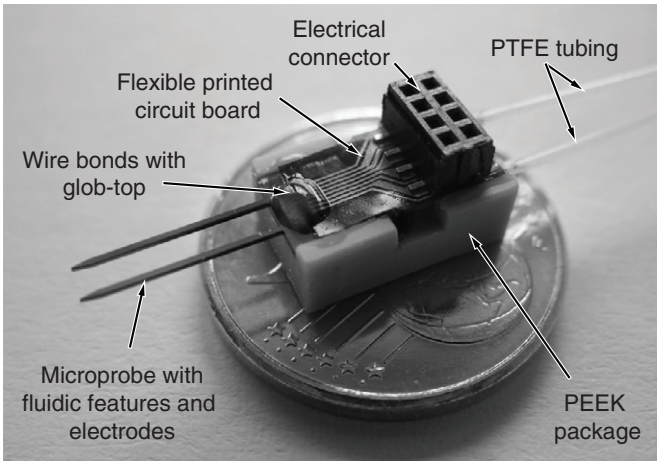


**Figure 8.** Fluidic probe assembly for drug delivery and simultaneous electric recordings.

However, forces acting perpendicularly to the shaft surface lead to probe fracture at much lower values. In order to estimate tolerable force levels, probe shafts were subjected to orthogonal forces applied close to the probe tips. A probe shaft with two integrated channels bent at a rate of 10 $\mu$m s$^{-1}$ survived deflections up to 0.3 mm corresponding to a load of 110 mN.

In order to evaluate the mechanical strength of the bonding process and the maximum pressure applicable to individual channels, probes without fluidic outlet ports were pressurized up to 9 bar with air and dipped into a water container for inspection. Since no gas bubbles were formed on the outer surface of the probes, it was concluded that the channels are gas tight up to a pressure of at least 9 bar. The silicon probes themselves were not destroyed at this pressure level.

### *4.2. Insertion behavior*

The experimental setup consisting of a commercial tensile tester (Zwick, Ulm, Germany) employing a piezoresistive force sensor with an accuracy of 0.5 mN and a maximum force of 5 N (KD40S, ME-Systeme, Henningsdorf, Germany) was applied to characterize the insertion behavior of the fluidic probes [49]. For this purpose, probes were inserted in 0.6% agarose gel covered by a polyethylene (PE) foil as a realistic model for the cortex and pia mater. The fluidic probes were inserted at a speed of 100 mm min$^{-1}$. On average, an insertion force of 120 $\pm$ 13 mN was derived from 43 measurements. In comparison, two-shaft combs with a shaft thickness of 100 $\mu$m and an inter-shaft pitch of 550 $\mu$m as described in [9] showed an insertion force of 78 mN [49]. The increased penetration force of the fluidic probes is caused by the larger probe thickness of 250 $\mu$m compared to 100 $\mu$m of the non-fluidic probes. Note that the tip opening angle of 17° is the same for both probe types. In addition, the observed dimpling of the foil and the agarose gel of 1.1 mm in comparison to 0.6 mm reported for the thinner non-fluidic probes [49] reflects the increased insertion forces. *In vivo* experiments have demonstrated the capability of these devices to penetrate the dura mater of rats [43].

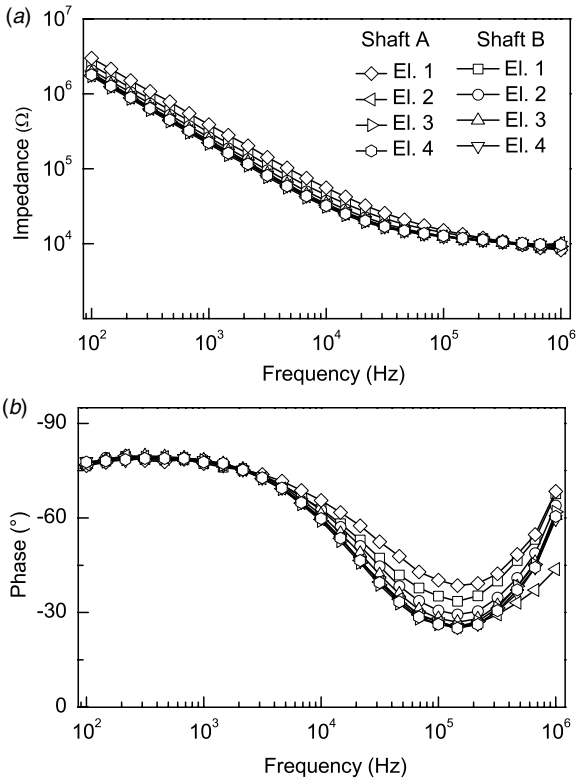


**Figure 9.** Frequency-dependent impedance (*a*) magnitude and (*b*) phase of the eight Pt-gray electrodes with a diameter of 20 $\mu$m located on two shafts of a fluidic microprobe.

### *4.3. Electrical characterization*

Electrical impedance spectra of the recording electrodes of individual microprobes are determined in Ringer's solution using a three-electrode setup with a Pt counter electrode and an Ag/AgCl reference electrode. At 1 kHz typical impedances of (1.8 $\pm$ 0.3) M$\Omega$ were determined for the Pt electrodes with a diameter of 20 $\mu$m. If required, the electrode impedance has been decreased by an additional deposition of Pt-black or Pt-gray using electroplating as described elsewhere [9, 13]. In the case of Pt-gray electrode metallization, the average electrode impedance at 1 kHz was reduced to 260 $\pm$ 59 k$\Omega$. Figure 9 shows the impedance spectra between $10^2$ Hz and $10^6$ Hz of all eight Pt electrodes of a fluidic probe with two shafts after the deposition of a Pt-gray layer [13]. The average spreading resistance of the electrode–electrolyte interface is 12 k$\Omega$. This value has been determined at the frequency of 145 kHz where the impedance phase angle is closest to 0° and where consequently the interface is most similar to a pure resistance [50]. It is in agreement with previously measured values [9]. Below this frequency, the spectra show the well-known capacitive behavior of the interface.

### *4.4. Fluidic characterization*

The microprobes were validated fluidically by attaching silicone tubing to the in-plane fluidic ports. The tubes were connected to a conventional syringe pump and colored solutions were dispensed into water. As an example,

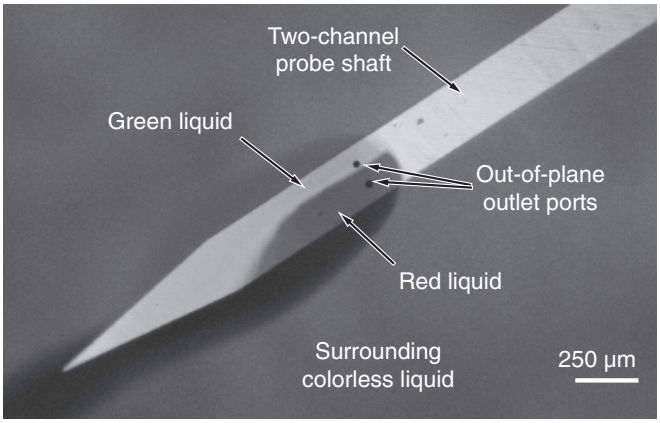


**Figure 10.** Simultaneous release of two different colored liquids from a two-channel probe shaft into water.

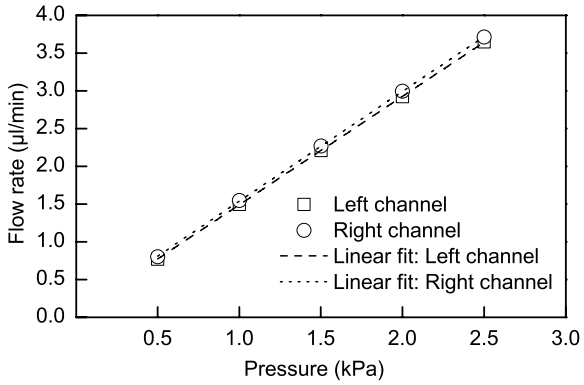


**Figure 11.** Average flow rates versus applied pressure for the left and right channels of a microfluidic probe (deionized, filtered and degassed water at 26 °C), with linear fits of the data.

figure 10 shows the simultaneous release of two differently colored liquids from a two-channel probe shaft. The fluidic characterization of the probes was performed by applying a hydrostatic pressure and measuring the resulting liquid flow rate with a commercial flow sensor ($\mu$-FLOW, Bronkhorst Mättig GmbH, Kamen, Germany). Figure 11 shows representative measurements for two channels of a microprobe. As expected from laminar flow theory, the flow–pressure relationship is linear. Further, the flow rate of the two channels differs only by 3% at 1.5 kPa corroborating the homogeneity of the fabrication process. Although the smallest microfluidic features of a microprobe, i.e. the outlet ports, have a diameter of 25 $\mu$m, a modest pressure of 1 kPa is sufficient to achieve a flow rate of 1.5 $\mu$L min$^{-1}$.

## 5. Discussion and conclusion

This paper presented the layout and fabrication of fluidic microprobes for simultaneous drug delivery and neural recording. The fabrication process is based on two-stage DRIE combined with silicon wafer bonding and grinding to realize channel structures. This technology has several advantages over previously reported approaches. As the fluidic structures are realized on a separate wafer independent of the cover wafer, the process offers considerable flexibility in the design of the fluidic channels. The channels have a cross-sectional area of $50 \times 50$ $\mu$m$^2$ along a shaft length of 8 mm. Up to two channels are integrated in one shaft. Previously reported neural probes with combined fluidic and recording capability used mainly bulk micromachining of the channels based on EDP and KOH wet etching [27, 28]. Their cross-sectional areas depend on the diffusion-limited etch rate and are therefore slightly smaller but still compatible with the presented work. However, the technology used for these channels imposes significant constraints on channel layout.

Further, the novel probe concept reported here enables both in-plane and out-of-plane fluidic supply of the neural probes to be realized. The resulting neural probes are intended equally for future platform integration and for stand-alone use. In contrast, the platform integration [17] with channels based on surface micromachining [19, 23–26] is more challenging due to the lacking top surface planarity. The current integration of outlet ports in the sidewalls of probe shafts and into the front of the cover wafer is a useful feature for neuroscientific experiments and thus represents a further advantage of the new concept over the previous approaches.

Structuring the probe shape by DRIE allows robust batch fabrication and allows higher stability of probe shanks compared to wet etching of boron-doped shanks [27]. Furthermore, structuring of silicon by DRIE is a CMOS-compatible process and thus allows in principle to integrate electronics even on the probe shaft [10]. In comparison to the DRIE-based approach based on SOI [37], the used standard silicon wafers are less costly. Probes fabricated of polymers such as SU-8 and parylene [32, 35] are more flexible, but are also more difficult to insert into brain tissue. In contrast, the presented fluidic probes are able to penetrate the pia and even the dura mater.

In addition to the microfluidic features, the probes also comprise electrodes, bonding pads and interconnection leads. In the current implementation, four electrodes are located around the outlet ports for simultaneous recording of electrical neural signals. Only a few approaches of other research groups offer this combined functionality on a microprobe [27, 28, 31, 32, 34]. The electrodes of our microprobes were electrochemically characterized and showed typical impedances of $1.8 \pm 0.3$ MΩ at 1 kHz for smooth Pt and $260 \pm 59$ kΩ with Pt-gray deposition. Previous experiments have demonstrated the capability of these electrodes for stable *in vivo* recordings [9, 43].

The microprobes were validated fluidically. Typical flow rates for neuroscience applications of 1.5 $\mu$L min$^{-1}$ are achieved at a low differential pressure of 1 kPa. The resulting flow resistivity is lower than in the case of other approaches. Flow rates of 16.7 $\mu$L min$^{-1}$ at 30 kPa [26], 50 $\mu$L min$^{-1}$ at 260 kPa [28], 11.7 $\mu$L min$^{-1}$ at 60 kPa [32], 0.2 $\mu$L min$^{-1}$ at 1 kPa [35] and 0.7 $\mu$L min$^{-1}$ at 137 kPa [38] have been reported in the literature. Further, our fluidic microprobes are gas tight up to a pressure of at least 9 bar, which is more than sufficient.

Experiments are currently being performed using the fluidic microprobes where pharmacologically active

substances are locally injected into several animal models while SUA and LFP are recorded [43]. Interfacing the brain both electrically and chemically opens new perspectives for neuroscientific research and applications such as the treatment of neurodegenerative brain diseases. Options for further developments include the combination of the fluidic probes with a fluidic actuation mechanism [51], their integration into the *NeuroProbes* modular platform [17], and the integration of biosensors directly on the fluidic microprobes so that the fluidic channels can be used to calibrate the biosensors *in vivo* [11].

## Acknowledgments

The authors gratefully acknowledge Kai Hiltmann and Axel Schumacher (both HSG-IMIT) for implementation of the system assembly, Neda Hosseini (IMTEK-MML) for performing insertion experiments, Armin Baur and Michael Reichel (both IMTEK-RSC) for useful discussions and technical support during cleanroom fabrication, Johannes Auber and the cleanroom team at HSG-IMIT for wafer processing and process optimization. This work was financially supported by the Information Society Technologies (IST) Integrated Project *NeuroProbes* of the 6th Framework Program (FP6) of the European Commission (project number IST-027017).

## References

[1] Pena F and Tapia R 2000 Seizure and neurodegeneration induced by 4-aminopyridine in rat hippocampus *in vivo*: role of glutamate- and GABA-mediated neurotransmission and of ion channels *Neuroscience* **101** 547–61

[2] Murphy E R, Dalley J W and Robbins T W 2005 Local glutamate receptor antagonism in the rat prefrontal cortex disrupts response inhibition in a visuospatial attentional task *Psychopharmacology* **179** 99–107

[3] Shain W, Spataro L, Haberstraw K, Dilgen J, Retterer S, Spence A, Isaacon M and Turner J 2003 Controlling cellular reactive responses around neural prosthetic devices using peripheral and local intervention strategies *IEEE Trans. Rehabil. Eng.* **11** 186–8

[4] Marin G, Letelier J C, Sentis E, Karten H, Mrosko B and Mpodozis J 2001 A simple method to microinject solid neural tracers into deep structures of the brain *J. Neurosci. Methods* **106** 121–9

[5] Frey O, Holtzman T, McNamara R M, Theobald D E H, van der Wal P D, de Rooij N F, Dalley J W and Koudelka-Hep M 2010 Simultaneous neurochemical stimulation and recording using an assembly of biosensor silicon microprobes and SU-8 microinjectors *Sensors Actuators* **B** at press (10.1016/j.snb.2010.01.034)

[6] Csicsvari J, Henze D A, Jamieson B, Harris K D, Sirota A, Barth P, Wise K D and Buzski G 2003 Massively parallel recording of unit and local field potentials with silicon-based electrodes *J. Neurophysiol.* **90** 1314–23

[7] Blanche T J, Spacek M A, Hetke J F and Swindale N V 2005 Polytrodes: high-density silicon electrode arrays for large-scale multiunit recording *J. Neurophysiol.* **93** 2987–3000

[8] Kelly R C, Smith M A, Samonds J M, Kohn A, Bonds A B, Movshon J A and Lee T S 2007 Comparison of recordings from microelectrode arrays and single electrodes in the visual cortex *J. Neurosci.* **27** 261–4

[9] Herwik S, Kisban S, Aarts A A A, Seidl K, Girardeau G, Benchenane K, Zugaro M B, Wiener S I, Paul O and Ruther P 2009 Fabrication technology for silicon-based microprobe arrays used in acute and sub-chronic neural recording *J. Micromech. Microeng.* **19** 074008

[10] Seidl K, Herwik S, Nurcahyo Y, Torfs T, Keller M, Schuettler M, Neves H P, Stieglitz T, Paul O and Ruther P 2009 CMOS-based high-density silicon microprobe array for electronic depth control on neural recording *Tech. Digest IEEE MEMS Conf. 2009 (Sorrento, Italy)* pp 232–5

[11] Frey O, van der Wal P, de Rooij N and Koudelka-Hep M 2007 Development and characterization of choline and L-glutamate biosensor integrated on silicon microprobes for *in-vivo* monitoring *Proc. 29th Ann. Int. IEEE EMBS Conf. 2007 (Lyon, France)* pp 6039–42

[12] Najafi K, Wise K D and Mochizuki T 1985 A high-yield IC-compatible multichannel recording array *IEEE Trans. Electron Devices* **32** 1206–11

[13] Kisban S, Herwik S, Seidl K, Rubehn B, Umilta M A, Stieglitz T, Paul O and Ruther P 2007 Microprobe array with low impedance electrodes and highly flexible polyimide cables for acute neural recording *Proc. 29th Ann. Int. IEEE EMBS Conf. 2007 (Lyon, France)* pp 175–8

[14] Vetter R J, Miriani R M, Casey B E, Kong K, Hetke J F and Kipke D R 2005 Development of a microscale implantable neural interface (MINI) probe system *Proc. 27th Ann. Int. IEEE EMBS Conf. 2005 (Shanghai, People's Republic of China)* pp 7341–44

[15] Olsson R H III and Wise K D 2005 A three-dimensional neural recording microsystem with implantable data compression circuitry *IEEE J. Solid-State Circuits* **40** 2796–804

[16] Bhandari R, Negi S, Rieth L, Normann R A and Solzbacher F 2007 A novel method of fabricating convoluted shaped electrode arrays for neural and retinal prosthesis *Tech. Digest IEEE TRANSDUCERS Conf. 2007 (Lyon, France)* pp 1231–4

[17] Aarts A A A, Neves H P, Puers R P and Van Hoof C 2008 An interconnect for out-of-plane assembled biomedical probe arrays *J. Micromech. Microeng.* **18** 064004

[18] Perlin G E and Wise K D 2009 Ultra-compact integration for fully-implantable neural microsystems *Tech. Digest IEEE MEMS Conf. 2009 (Sorrento, Italy)* pp 228–3

[19] Neeves K B, Lo C T, Foley C P, Saltzman W M and Olbricht W L 2006 Fabrication and characterization of micro fluidic probes for convection enhanced drug delivery *J. Control. Release* **111** 252–62

[20] Kliem M A and Wichmann T A 2004 Method to record changes in local neuronal discharge in response to infusion of small drug quantities in awake monkeys *J. Neurosci. Methods* **138** 45–9

[21] Tokuno H, Hatanaka N, Chiken S and Ishizuka N 2002 An improved method with a long-shanked glass micropipette and ultrasonography for drug injection into deep brain structure of the monkey *Brain Res. Protoc.* **10** 16–22

[22] Rohatgi P, Langhals N B, Kipke D R and Patil P G 2009 *In vivo* performance of a microelectrode neural probe with integrated drug delivery *Neurosurg. Focus* **27** E8

[23] Lin L and Pisano A P 1999 Silicon-processed microneedles *J. Microelectromech. Syst.* **8** 78–84

[24] Retterer S T, Smith K L, Bjornsson C S, Neeves K B, Spence A J H, Turner J N, Shain W and Isaacson M S 2004 Model neural prostheses with integrated microfluidics: a potential intervention strategy for controlling reactive cell and tissue responses *IEEE Trans. Biomed. Eng.* **51** 2063–73

[25] Papautsky I, Brazzle J, Swerdlow H and Frazier A B 1998 A low-temperature IC-compatible process for fabricating surface-micromachined metallic microchannels *J. Microelectromech. Syst.* **7** 267–73

[26] Chandrasekaran S, Brazzle J D and Frazier A B 2003 Surface micromachined metallic microneedles *J. Microelectromech. Syst.* **12** 281–88
[27] Chen J, Wise K D, Hetke J F and Bledsoe S C 1997 A multichannel neural probe for selective chemical delivery at the cellular level *IEEE Trans. Biomed. Eng.* **44** 760–9
[28] Cheung K C, Djupsund K, Dan Y and Lee L P 2003 Implantable multichannel electrode array based on SOI technology *J. Microelectromech. Syst.* **12** 179–84
[29] de Boer M J, Tjerkstra R W, Berenschot J W, Jansen H V, Burger G J, Gardeniers J G E, Elwenspoek M and van den Berg A 2000 Micromachining of buried micro channels in silicon *J. Microelectromech. Syst.* **9** 94–103
[30] Dijkstra M, de Boer M J, Berenschot J W, Lammerink T S J, Wiegerink R J and Elwenspoek M 2007 A versatile surface channel concept for micro fluidic applications *J. Micromech. Microeng.* **17** 1971–7
[31] Paik S J, Lee A R, Koo K I, Park S K, Jeong M J, Choi H M, Lim J M, Oh S J, Kim S J and Cho D I 2005 Localized stimulation and recording from neural cells with fluid injectable neuronal microneedles *Proc. 9th Int. MicroTAS Conf. 2005 (Boston, MA, USA)* vol 2 pp 1177–9
[32] Fernandez L J, Altuna A, Tijero M, Gabriel G, Villa R, Rodraguez J, Batlle M, Vilares R, Berganzo J and Blanco F J 2009 Study of functional viability of SU-8 based microneedles for neural applications *J. Micromech. Microeng.* **19** 025007
[33] Parker E R, Rao M P, Turner K L, Meinhart C D and MacDonald N C 2007 Bulk micromachined titanium microneedles *J. Microelectromech. Syst.* **16** 289–95
[34] Park S, Jang Y, Kim H C and Chun K 2008 Fabrication of drug delivery system with piezoelectric micropump for neural probe *Proc. 23rd Int. Tech Conf. on Circuits/Systems, Computers and Communications 2008 (Yamaguchi, Japan)* pp 1149–52
[35] Ziegler D, Suzuki T and Takeuchi S 2006 Fabrication of flexible neural probes with built-in microfluidic channels by thermal bonding of parylene *J. Microelectromech. Syst.* **15** 1477–82
[36] Vrouwe E, Kelderman A J and Blom M 2008 Microfluidic glass needle arrays for drug dosing during neural recording *Proc. 12th Int. MicroTAS Conf. 2008 (San Diego, CA, USA)* pp 378–80
[37] Sparks D and Hubbard T 2004 Micromachined needles and lancets with design adjustable bevel angles *J. Micromech. Microeng.* **14** 1230–3
[38] Zahn J D, Talbot N H, Liepmann D and Pisano A P 2000 Microfabricated polysilicon microneedles for minimally invasive biomedical devices *Biomed. Microdevices* **2** 295–303
[39] Neves H, Orban G, Koudelka-Hep M, Stieglitz T and Ruther P 2007 Development of modular multifunctional probe arrays for cerebral applications *Proc. 3rd Int. IEEE EMBS Conf. on Neural Eng 2007 (Kohala Coast, HI, USA)* pp 104–9
[40] Ruther P *et al* 2008 The NeuroProbes project—multifunctional probe arrays for neural recording and stimulation *Biomed. Technol. Proc. 13th Ann. Int. FES Soc. Conf. 2008 (Freiburg, Germany)* **53** 238–40
[41] Ruther P, Herwik S, Kisban S, Seidl K and Paul O 2010 Recent progress in neural probes using silicon MEMS *IEEJ Trans EIS* **5** 1–11
[42] Seidl K, Spieth S, Steigert J, Paul O and Ruther P 2007 Fabrication process for silicon in-plane probes for simultaneous neural recording and drug delivery *Book of Abstracts, 7th Int. Workshop on High-Aspect-Ratio Micro-Structure Technology (HARMST) (Besançon, France)* pp 247–8
[43] Spieth S, Schumacher A, Seidl K, Hiltmann K, Haeberle S, McNamara R, Dalley J W, Edgley S A, Ruther P and Zengerle R 2008 Robust microprobe system for simultaneous neural recording and drug delivery *Proc. 4th Eur. IFMBE Conf. 2008 (Antwerp, Belgium)* vol 22 pp 2426–30
[44] Meyer J-U, Stieglitz T, Scholz O, Haberer W and Beutel H 2001 High density interconnects and flexible hybrid assemblies for active biomedical implants *IEEE Trans. Adv. Pack.* **24** 366–74
[45] Jansen H, De Boer M, Wiegerink R, Tas N, Smulders E, Neagu C and Elwenspoek M 1997 RIE lag in high aspect ratio trench etching of silicon *Microelectron. Eng.* **35** 45–50
[46] Malyshev M V and Donnelly V M 2000 Bias-plasma interaction in pulsed plasmas and its relation to damage mechanisms *Proc. 5th Int. Symp. on Plasma Process-Induced Damage 2000 (Santa Clara, CA, USA)* pp 18–21
[47] Ahn T H, Nakamura K and Sugai H 1996 Negative ion measurements and etching in a pulsed-power inductively coupled plasma in chlorine *Plasma Sources Sci. Technol.* **5** 139–44
[48] Hopkins J, Johnston I R, Bhardwaj J K, Ashraf H, Hynes A M and Lea L M 2001 Method and apparatus for etching a substrate *US Patent 6187685*
[49] Haj Hosseini N, Hoffmann R, Kisban S, Stieglitz T, Paul O and Ruther P 2007 Comparative study on the insertion behavior of cerebral microprobes *Proc. 29th Ann. Int. IEEE EMBS Conf. 2007 (Lyon, France)* pp 4711–4
[50] Mercanzini A, Colin P, Bensadoun J-C, Bertsch A and Renaud P 2009 *In vivo* electrical impedance spectroscopy of tissue reaction to microelectrode arrays *IEEE Trans. Biomed. Eng.* **56** 1909–18
[51] Spieth S, Schumacher A, Kallenbach C, Messner S and Zengerle R 2010 Neuromedicator—a disposable drug delivery system with silicon microprobes for neural research *Tech. Digest MEMS Conf. 2010 (Hong Kong, People's Republic of China)* pp 983–6